Received August 13, 2020, accepted September 10, 2020, date of publication September 21, 2020,
date of current version September 30, 2020.

Digital Object Identifier 10.1109/ACCESS.2020.3025309

Frame-Angle Controlled Wavelet Modulated Inverter and Self-Recurrent Wavelet Neural Network-Based Maximum Power Point Tracking for Wind Energy Conversion System

TEENA GEORGE[1], (Member, IEEE), P. JAYAPRAKASH[1], (Senior Member, IEEE), UMASHANKAR SUBRAMANIAM[2], (Senior Member, IEEE), AND DHAFER J. ALMAKHLES[2], (Senior Member, IEEE)

[1]Department of Electrical and Electronics Engineering, Government College of Engineering Kannur, A. P. J. Abdul Kalam Technological University, Thiruvananthapuram 695016, India

[2]Renewable Energy Laboratory, Department of Communications and Networks Engineering, Prince Sultan University, Riyadh 11586, Saudi Arabia

Corresponding author: Teena George (teena.g87@gmail.com)

This work was supported in part by the Centre of Excellence in Systems Energy and Environment (CESEE), Government College of Engineering, Kannur, India, and in part by the Renewable Energy Research Lab, College of Engineering, Prince Sultan University, Riyadh, Saudi Arabia.

ABSTRACT In this work, a new control methodology is proposed for Type -IV wind energy conversion system (WECS) using a self-recurrent wavelet neural network (SRWNN) control with a Vienna rectifier as the machine side converter (MSC). A SRWNN combines excellent dynamic properties of recurrent neural networks and the fast convergence speed of wavelet neural network. Hidden neurons of SRWNN contains local self-feedback loops, which provide the memory feature and the necessary information of past values of the signals, allowing it to track maximum power from WECS under varying wind speeds. The Vienna rectifier allows unity power factor operation to increase electrical efficiency. Frame angle-controlled wavelet modulation is proposed for the grid side converter (GSC). Wavelet modulated inverter produces output voltage fundamental components with higher magnitudes than those obtained from the pulse width modulated inverters. The non-linear load compensation and power quality enhancement are achieved by executing frame angle control for WM inverter. The overall system is modeled, and performance is verified in MATLAB Simulink. The hardware prototype is developed, and the switching pulses for the rectifier and inverter are generated using dSPACE1104 controller. The results prove that the system provides low harmonic content and high magnitude of the fundamental current component at the machine and grid sides and ensures maximum power operation at various wind speeds.

INDEX TERMS Wind energy conversion system (WECS), wavelet modulation (WM), maximum power point tracking (MPPT), self-recurrent wavelet neural network (SRWNN).

I. INTRODUCTION

As the wind power generation has been increasing day by day,it is essential to design and select a proper generator and converters for wind energy conversion system (WECS). Power converters are the backbone of WECS for interfacing with the grid to provide greater flexibility in their operation and control, both during steady-state and transient conditions [1]. Various power converter topologies have been proposed in the literature for the variable-speed permanent magnet synchronous generator based WECS. With the advantages of low cost, high reliability, and simple control algorithms, a simple configuration integrating a diode rectifier, a DC chopper, and a voltage source inverter (VSI) is widely adopted [2]. However, with the increasing power level of the WECS, the power switch device of a DC chopper in the topology must endure high instantaneous voltage and current stress [3]. A two-level back-to-back topology with two pulse

The associate editor coordinating the review of this manuscript and approving it for publication was Xiaowei Zhao.

width modulated (PWM) converters connected by a storage capacitor, that connects the generator to the grid is used to reduce input current harmonics and results ripple-free electromagnetic torque [4]. The machine side converter (MSC) of back-to-back converter will control the generator speed and electromagnetic torque and GSC regulates the power flow to the grid in order to keep the DC-link voltage constant and reduce the total harmonic distortion (THD). Back-to-back multi-level converters (MLC) was discussed in [5] for high power WECS. MLCs allows lower harmonic distortion and operation at a higher DC voltage, but it requires complex control. There is the chance of capacitors, voltage unbalance, and an increased number of switches. Matrix converter (MC) has also received increasing attention in recent years as it avoids the DC-link stage but requires complex control to ensure proper control at both generator and grid side which are not entirely decoupled [6]. To provide better control with a reduced number of switches and with low cost, a three phase-three switch-three level rectifier called Vienna rectifier is used as MSC [7]. Vienna rectifier generates three voltage levels with three power switches, thus simplifying the control, provides high input current quality, lower torque ripple, lower voltage stresses on switches which can enhance reliability and improved power factor [8]. In [9] Vienna rectifier is controlled, to function as a parallel active filter. In [10], a fuzzy logic-based control is proposed for Vienna rectifier instead of conventional PI control.

The function of MSC is to ensure maximum power tracking and improve generator current quality to reduce the electromagnetic torque ripples. There are different control algorithms and maximum power tracking methods. The two most dominant control strategies are field-oriented control (FOC) and direct torque control (DTC) having a similar dynamic response [11]. In FOC, a linear relationship between the stator currents and electromagnetic torque are used and is realised using PI controllers. Hence the performance of FOC depends on the tuning of PI controller. In [12] a modified fractional order PI controller and a direct power control algorithm are used. In DTC avoids the dependency of the decoupled current control on machine parameters,but its switching frequency changes with operating conditions and relatively high ripples in the flux and torque [13]. To reduce this space vector modulation is integrated along with DTC [14]. A full order sliding-mode observer is used to estimate the rotor position and flux, which makes the system work at a fixed switching frequency [13]. For large scale WECS DTC will not show sufficient performance. When these controllers perform MPPT, the use of wind speed sensors and rotor speed/position sensors increase the system cost and size [15]. The main categories of MPPT control algorithms are tip speed ratio (TSR)control, optimum relationship-based (ORB) control, and hill climb search control (HCS) (or perturb and observe) [15]–[17]. The conventional TSR control gives higher accuracy by using anemometers to measure wind speed. To avoid uncertainties in wind, a neural network-based generalized global sliding mode controller is proposed along with TSR [17]. In [18], TSR and ORB with optimum torque are compared. According to the authors, TSR gives a fast response, while ORB gives smooth power output. HCS method with a fixed-step size is prevalent due to its simple algorithm but it causes oscillations near MPP and directionality problem for a sudden increase in wind speed. A fuzzy-logic-based HCS algorithm is discussed in [19] to evade these disadvantages. Nevertheless, the range of operation is limited in the HCS method [15]. ORB control requires field tests for each WECS to obtain the optimum relationship, even though it is simple with fast response. A Particle Swarm Optimization-based MPPT method is proposed by M. A. Abdullah and et.al., to avoid wind speed sensors and prior knowledge of system parameters [20], but it causes electromagnetic torque ripples. A hybrid fuzzy particle swarm optimisation-based algorithm is employed to obtain high tracking efficiency in [21]. Predictive control algorithms are useful in steady-state operation [22], but during the transient changes, it exhibits an inadequate response due to mismatch of memorized data [23]. Sliding mode observer for measuring rotor speed and torque of PMSG is reported in [24], even though it avoids mechanical sensors, the complexity of such controllers is comparatively higher than that of intelligent control algorithms such as neural network, fuzzy logic, wavelet controllers etc. Chattering problem of sliding mode observer also reduces the reliability of the system. On this basis, it should be emphasised that artificial neural network(ANN) based intelligent controller [25], [26] has a fast dynamic response, less sophisticated design and less reliance on parameters of WECS. A wavelet neural network (WNN) has a nonlinear regression structure that uses the localized basis functions in its hidden layer for achieving the desired input-output mapping. This makes WNN a superior system model than ANN and has been used by researchers for solving various approximation, control, prediction, and classification type of problems [27]. A comparative analysis of different MPPT algorithms and its features along with the proposed method is illustrated in Table 1. At the grid side, better control techniques are needed to supply available power to the load/grid and to improve the power quality. To date, the voltage source converter is prevalent to integrate grid with renewable energy networks due to its flexibility in controlling. Different control algorithms proposed many researchers to satisfy the targeted control goals. A model predictive control (MPC) with a finite control set is reported in [28]. The system response time is reduced,as the cost function is designed only for current controller tracking. A lookup-table-based weighting factor design is proposed for cost function of MPC control in [29], which reduces the switching frequency less than 1kHz. A fixed switching frequency operation with MPC algorithms is analysed for a grid connected inverter [30]. Based on minimisation of the cost function of MPC, an optimum voltage vector is generated to activate modulator. High computational requirement of MPC is avoided by this. These schemes depend on the model of the system and there is a lack of flexibility during steady

TABLE 1. Comparison of MPPT methods for WECS.

MPPT Features	TSR [17]	ORB [20]	HCS [16]	Fuzzy [19]	ANN [25]	Proposed SRWNN
Requirement of wind speed sensor	Yes	Yes	No	Depends	Depends	No
Requirement of shaft speed sensor	Yes	Yes	Yes	Depends	Depends	No
Requirement of system pre-knowledge	No	Yes	No	Depends	Depends	Yes
Memory Requirement	No	Yes	No	Yes	Yes	Yes
Convergence Speed	Very Fast	Fast	Slow	Moderate	Moderate	High
Oscillation at MPP and directionality problem	Low	Low	High	Very low	Very low	Very Low
Performance under fluctuating wind speed	Moderate	Moderate	Poor	Fast	Fast	Fast

state and transient conditions. Sliding mode control (SMC) approach is used to secure a fast dynamic response [31], [32]. A feed-forward negative sequence voltage is used in the vector current control in [31]. In [32] an adjustable reaching law is presented for gain correction. Even though total harmonic distortion (THD) reduced to a certain, but the control fails in case of unmatched uncertainties. Space vector modulation for the voltage source inverter (VSC) requires current compensator; broadly PI controller works this function. Tuning of PI control for varying grid condition with non-linear is difficult. Fuzzy space vector pulse width modulation method of current control is reported in [21] replacing PI control. Second order generalised integral (SOGI) based control algorithm is utilized to evaluate fundamental component of load current by using a feedback loop to estimate the phase and frequency of input signal in [33]. To reduce the effect of grid voltage dc offset in SOGI, a mixed second and third-order generalized integrator phase-locked loop is proposed in [34]. The available controllers are based on pulse width modulated (PWM) inverter, where output harmonic distortion affects the performance of controller [35]. Wavelet modulated (WM) inverters showed improved performance in terms of high amplitude of fundamental component and less harmonic contents [36], [37]. A grid connected WECS with resolution level control approach for WM inverter is implemented in [35] in which, sampling is done based on an integer value. In order to avoid this problem frame angle-based approach is used for grid connected solar system in [38]. The WM and frame angle control are useful in compensating the harmonics, reactive power and regulating grid active power.

Motivated by the analysis, this paper proposes sef-recurrent wavelet neural network (SRWNN) MPPT control at MSC and frame angle control with wavelet modulation at GSC for a PMSG driven WECS. At the grid side,frame angle control is proposed with WM inverter. The frame-angle control is based on controlling d-q axis voltage by regulating d-q axis current of GSC in response to available wind power and reactive power requirement of load. The phase shift angle θ obtained from reference d-q voltages is used to generate reference signals for the wavelet modulation. The key features of proposed system are,

- The MSC used is a Vienna rectifier which requires only one turn-off power semiconductor device (IGBT) per phase.
- Vienna rectifier allows a continuous, uninterrupted input current with comparably low switching frequency components, which reduces the electromagnetic torque ripples produced in the PMSG windings.
- SRWNN applied to Vienna rectifier performs MPPT operation without using mechanical sensors.
- The hidden neurons of SRWNN contain local self-feedback loops, provides it with the memory feature and the necessary information of past values of the signals. This feature allows SRWNN to handle time varying wind speeds.
- The Frame-angle control at GSC allows the system to supply available power to grid/load and also act as an active filter to compensate the reactive power requirements of load.

The unity power factor operation of Vienna rectifier and maximum power tracking of WNN control is verified at the machine side. The real power control, reactive power control and harmonic elimination are verified at the grid side.

The paper is organized in such a way that Section II gives the design of Vienna rectifier with sensor-less wavelet neural network controller proposed system and its description and Section III deals with the control of GSC. In Section IV shows the results and discussions of the proposed system and finally conclusion in section V.

II. DESIGN OF VIENNA RECTIFIER WITH SELF-RECURRENT WAVELET NEURAL NETWORK CONTROL

Appropriate sizing of the reactive elements is crucial for an active front-end converter instead of a passive diode bridge, which is typically to reduce the line current harmonics and unity power factor operation. For the same converter rating and harmonic specifications, the size of the three-level converter input inductor is smaller since the peak-to-peak ripple voltage seen by the inductor is half the dc bus voltage [39]. For wind power application with varying input frequency, Vienna rectifier is the best solution [25].

A schematic layout of Vienna rectifier with grid-connected WECS is shown in Fig. 1. The circuit configuration of the three-phase three-level Vienna rectifier composed of a three-phase diode bridge and three bidirectional switches connecting the input phases to the neutral point of the dc-bus as in Fig.1.

A. SRWNN CONTROL FOR MSC

WECS is a dynamic system with uncertainties in the values of their parameters. Therefore, conventional control methods based on the models are likely to fail in providing the desired

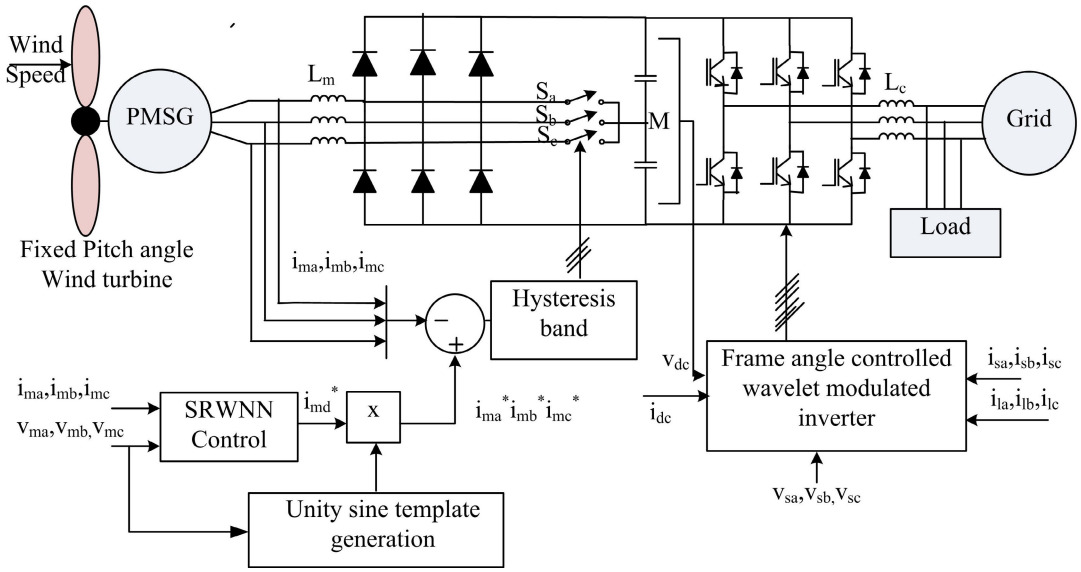

FIGURE 1. WECS connected to the grid through Vienna rectifier and frame angle controlled WM inverter.

performance. A WNN has a nonlinear regression structure that uses the localized basis functions in its hidden layer for achieving the desired input-output mapping. This makes WNN a superior system model than ANN and has been used by many researchers for solving various approximations, control, prediction, and classification type of problems. It combines the properties of RNN such as attractor dynamics and the fast convergence of WNN [27]. SRWNN hidden neurons contain local self-feedback loops, which provides it with the memory feature and the necessary information of past values of the signals, which allows it to handle the time-varying inputs, changes occurring in the control environment, etc. The presence of temporal feature makes SRWNN structure simple since a smaller number of neurons is required as compared to the WNN.

Fig.2. shows the structure of SRWNN. It consists of four layers. The first layer accepts the externally applied input signals and transmits them directly to the second layer. The second layer is the wavelet and recurrent layer.

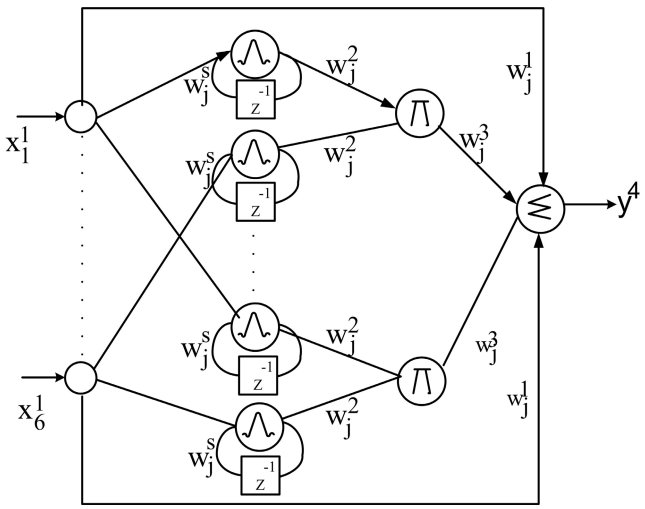

FIGURE 2. Structure of SRWNN for MSC.

Layer 1: Input Layer - Layer 1 consists of two nodes which are two inputs, the WECS machine side voltage Vwabc and machine side current iwabc. Nodes in layer 1 transmit the input signals to the layer 2. The input and output of ith node can be written as,

$$u_j^{(1)}(t) = x_j^{(1)}(t) \tag{1}$$

Layer 2: Recurrent Wavelet Layer- The second layer is the mother wavelet layer, where each node includes a mother wavelet and a self-feedback loop. In this paper the first derivative of the Gaussian function is selected as the mother wavelet function is given by

$$\psi(x) = -x \exp(-\frac{x^2}{2}) \tag{2}$$

The wavelet of each node jk could be transferred from the mother wavelet directly, as follows:

$$y^2(t) = \psi_{jk}(Z_{jk}(t)) = \psi(\frac{u_{jk}(t) - d_{jk}(t)}{m_{jk}(t)}) \tag{3}$$

$$Z_{jk}(t) = \frac{u_{jk}^{(2)}(t) - d_{jk}^{(2)}(t)}{m_{jk}(t)} \tag{4}$$

where the first subscript j denotes the wavelet position and the second subscript k denotes the neuron position in that wavelet. $u_{jk}^{(2)}(t)$ is the input at the second layer. Terms $d_{jk}(t)$ and $m_{jk}(t)$ denote the translational and dilation factor values, respectively. The input signal to any neuron consists of the signal coming from the input layer plus its own unit delayed weighted output, that is

$$u_j^{(2)}(t) = y_j^1(t) + w_j^s(t)\psi_{jk}(t-1) \tag{5}$$

Here, $w_j^s(t)$ represents the weighted self-feedback loop and $\psi_{jk}(t-1)$ gives memory in the past state.

Layer 3: Rule Layer - Each node in this layer represents one wavelet rule and performs precondition matching of a rule. Thus, the neuron in this layer is denoted by π, which multiplies the incoming signals from layer 2 and outputs the product result, i.e., the firing strength of a rule. For the j^{th} rule node:

$$y_j^{(3)}(t) = \prod_{1}^{n/2} y_j^{(2)}(t) w_j^2 \tag{6}$$

where $y_j^{(3)}(t)$ represents the output of layer 3 and w_j^2 are the weights between the wavelet layer and the rule and n is the number of rules.

Layer 4: Output Layer-The neuron in this layer gives net value of the incoming signals, which computes the overall output as the summation of all incoming signals, which are $y_j^{(3)}(t)$ from the output of layer 3 (rule layer). The output of the SRWNN $y^4(t)$ is given by

$$y^4(t) = \sum_{1}^{m} y_j^{(3)}(t) w_j^3 + \sum_{1}^{m} x_j^{(1)}(t) w_j^1 \tag{7}$$

where w_j^3 connection weights between the rule layer and the output layer. The output $y_j^{(4)}(t)$ will be the dc component of source current corresponding to maximum power output from the wind turbine.

B. LEARNING ALGORITHM FOR SRWNN

The online learning algorithm for constructing the SRWNN model consists of structural learning and a parameter learning algorithms. The structural learning based on degree measure method and parameter learning based on back propagation (BP) algorithm are used concurrently for training the SRWNN model. The structural learning algorithm is responsible for online wavelet bases generation. The parameters of the wavelet bases, feedback weights, and connection weights are adjusted by back propagation algorithm.

Initially, there are no wavelet bases in the SRWNN model. The first step is to decide when a new wavelet base is generated. For each incoming pattern x_i, the firing strength of a wavelet base can be considered as the degree of the incoming pattern belonging to the corresponding wavelet. An input pattern x_i with a higher firing strength indicates that its spatial location is nearer to the center of the wavelet base b_{ij} $(i = 1, \ldots, n; j = 1, \ldots, m)$, than those with smaller firing strength. Based on this, the firing strength obtained from $y_j^{(3)}(t)$ in the rule layer can be used as the degree measure. Based on this concept, the firing strength was obtained from Eq. (6) in the rule layer can be used as the degree measure.

$$F_j = |y_j^3| \tag{8}$$

where $j = 1, \ldots, n$, n is the number of existing wavelet bases, and $|y_j^3|$ is the absolute value of y_j^3.

For generating new wavelet base for a new incoming data, the steps are:

Step 1: Define a threshold value for the degree measure.

The threshold is set between zero and one. A low threshold value generates a smaller number of rules, whereas a high threshold value generates a larger number of rules. Therefore, the selection of the threshold value F_{th} will directly affect the results of dynamic response. In the structural learning for SRWNN, F_{th} is set to 0.45, after testing the system with different values between 0 and 1.

Step 2: Find the maximum degree F_{max}

$$F_{max} = max(F_j) \tag{9}$$

$j = 1, 2, \ldots n$

Step 3: Check whether $F_{max} \leq F_{th}$

If $F_{max} \leq F_{th}$, Then a new wavelet base is generated, where F_{th} is a pre-specified threshold that should decay during the learning process, limiting the size of the SRWNN model.

Step 4: Assign the initial translation and dilation to the new wavelet base and the corresponding weights for the links. The translation, dilation and weights are all adjustable in the parameter learning phase as our aim is to minimize an objective function. Hence, the translation, dilation and weights for the new wavelet base are set as below:

$$d_{jk}(t+1) = x_i(t) \tag{10}$$

$$m_{jk}(t+1) = m_{int} \tag{11}$$

$$w_j^s(t+1) = w_j^4(t+1) = w_j^3(t+1) = w_0 \tag{12}$$

where $x_i(t)$ is the new incoming data at time t; the connection weight of the output layer and feedback weights are initially selected as a random variable in the range between -1 and 1. The dilation factor is selected as m_{int} pre-specified constant.

Step 5: Continue step 3 and Step 4, till $F_{max} > F_{th}$

The structure of the SRWNN is adjusted by structural learning according to the current pattern, then the network begins to adjust the parameters of the SRWNN such as self-recurrent weight, connection weights, and feedback weight optimally with the same training pattern by using parameter learning method. In the parameter learning algorithm, the weights are updated so as to minimize the energy function. The output obtained from SRWNN is the dc component of source current corresponding to the maximum power output from the wind turbine.

The energy function is defined as the

$$E = \frac{1}{2}(i_{mq}^* - i_{mq})^2 = \frac{1}{2}(e)^2 \tag{13}$$

i_{mq}^* is the reference value of the dc component of the generator current and i_{mq} is its actual value. The flowchart for the SRWNN control algorithm is shown in Figure 3.

III. CONTROL OF GSC

When the WECS is connected to the grid through an inverter, it allows transferring of all available power from the WECS to the grid or load and with the proposed controller for inverter it can compensate the reactive power requirement of load and the harmonics present in non-linear loads connected to the grid. The inverter will transfer the maximum available power

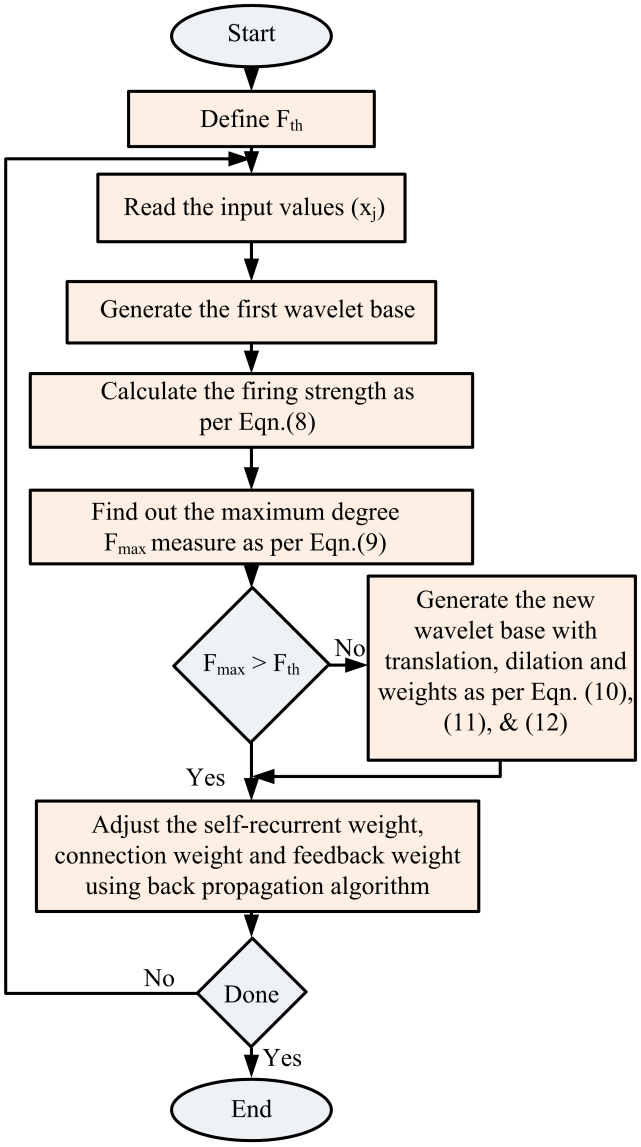

FIGURE 3. Flowchart of SRWNN control.

to the grid and also acts as an active filter to compensate the reactive power and makes the grid current at unity power factor with minimum total harmonic distortion. The GSC is connected to the point of common coupling (PCC) through a filter inductance L_f with resistance R_f, and the control block diagram is depicted in Fig. 3. The instantaneous values of active and reactive power injected to the grid from the GSC in terms of d-q axis components of voltage (v_d, v_q) and current injected by GSC (i_{wd}, i_{wq}) can be expressed as [20],

$$P = \frac{3}{2}(v_d i_{wd} + v_q i_{wq}) \tag{14}$$

$$Q = \frac{3}{2}(v_d i_{wq} + v_q i_{wd}) \tag{15}$$

The active power available in the WECS is

$$P = v_{dc} i_{dc} \tag{16}$$

To compensate the reactive power requirement of load, the reactive component current injected by GSC is to meet reactive component of load current (i_{lq}).

$$i^*_{wq} = i_{lq} \tag{17}$$

From equations (1) and (2) the reference value of the direct axis component of current injected by WECS is expressed as [40],

$$i^*_{wd} = \frac{2P}{3v_d} - \frac{v_q i_{lq}}{v_d} \tag{18}$$

The inverter used is a three-phase wavelet modulated inverter whose output voltage equations can be expressed in terms of three scale-based linearly combined synthesis scaling functions $(\psi_a(t)_j)$, $(\psi_b(t)_j)$, $(\psi_c(t)_j)$ as [41],

$$\frac{v_{wa}(t)}{v_{dc}} = \sum_{j=1}^{J}(\check{\psi}_a(t))_j + \sum_{j=1}^{J-1}(\check{\psi}_a(t))_{J-j}(t) - \sum_{j=1}^{J}(\check{\psi}_a(t))_j(t - \frac{T_m}{2}) - \sum_{j=1}^{J-1}(\check{\psi}_a(t))_{J-j}(t - \frac{T_m}{2}) \tag{19}$$

$$\frac{v_{wb}(t)}{v_{dc}} = \sum_{j=1}^{J}(\check{\psi}_b(t))_j + \sum_{j=1}^{J-1}(\check{\psi}_b(t))_{J-j}(t) - \sum_{j=1}^{J}(\check{\psi}_b(t))_j(t - \frac{T_m}{2}) - \sum_{j=1}^{J-1}(\check{\psi}_b(t))_{J-j}(t - \frac{T_m}{2}) \tag{20}$$

$$\frac{v_{wc}(t)}{v_{dc}} = \sum_{j=1}^{J}(\check{\psi}_c(t))_j + \sum_{j=1}^{J-1}(\check{\psi}_c(t))_{J-j}(t) - \sum_{j=1}^{J}(\check{\psi}_c(t))_j(t - \frac{T_m}{2}) - \sum_{j=1}^{J-1}(\check{\psi}_c(t))_{J-j}(t - \frac{T_m}{2}) \tag{21}$$

where $v_{wa}(t)$, $v_{wb}(t)$, $v_{wc}(t)$ are the voltages across the three legs of the inverter, v_{dc} is the inverter input dc voltage, T_m is the period of each reference modulating signal and J is the maximum value of the scale j as $J = max(j)$.
Applying voltage balance across grid filter,

$$v_{wd} = R_f i_{wd} + L_f \frac{di_{wd}}{dt} - \omega L_f i_{wq} + v_d \tag{22}$$

$$v_{wq} = R_f i_{wq} + L_f \frac{di_{wq}}{dt} - \omega L_f i_{wd} + v_q \tag{23}$$

Another input is δ obtained from phase-locked loop, which is used to generate reference modulating signals for three phases $S_{ga}(t)$, $S_{gb}(t)$, $S_{gc}(t)$.

A. THREE-PHASE WAVELET MODULATION TECHNIQUE

Wavelet modulation technique is a switching technique for power electronic converter based on non-uniform recurrent sampling-reconstruction of reference signals. This method has advantages like simple implementation, high magnitude

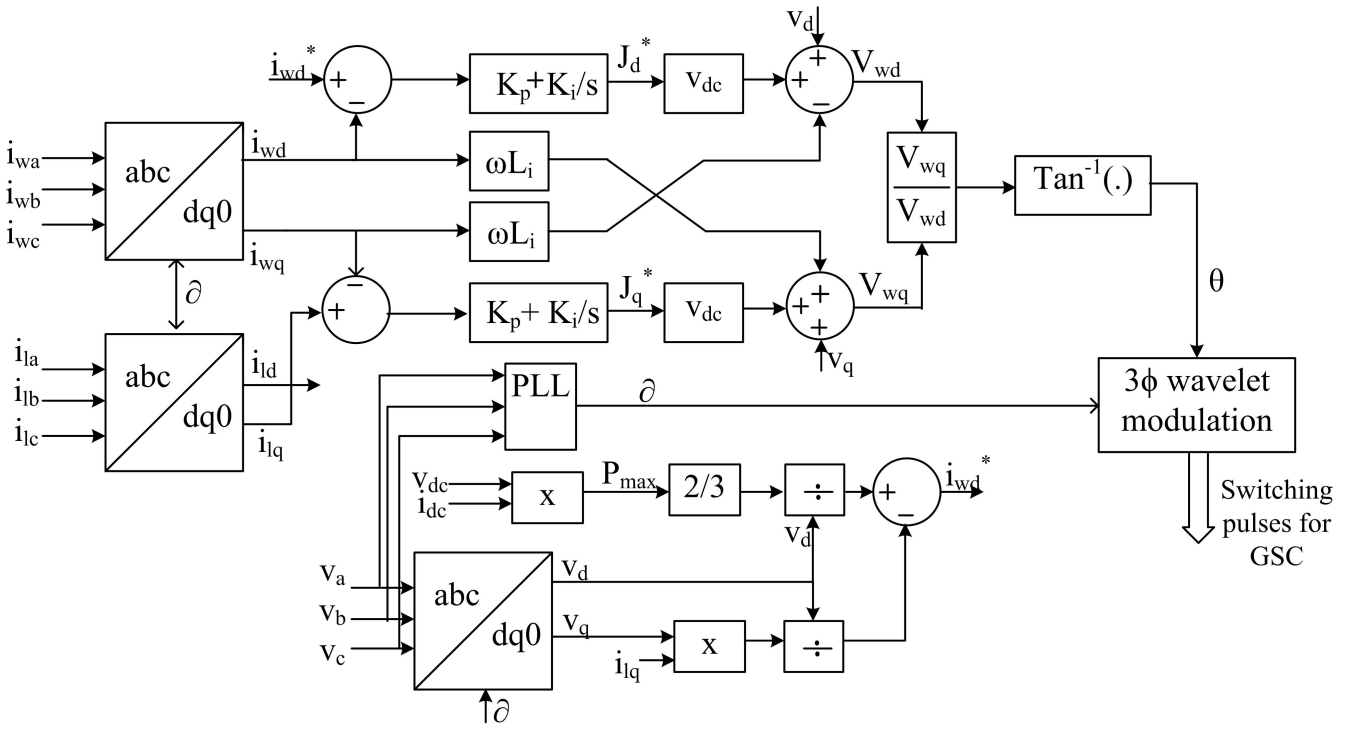

FIGURE 4. Frame angle control of WM inverter of proposed WECS.

of the output fundamental components, low harmonic contents of output, low switching losses, as compared to other modulation techniques [38]. Wavelet modulation technique is achieved by constructing nondyadic-type multi-resolution analysis, having two parts. The analysis part is for creating groups of non-uniform recurrent samples from the reference modulating signal, where each group has two samples. These groups of samples are created using sets of dilated and shifted versions of the scale-based linearly-combined basis functions $\psi_a(t)$, $\psi_b(t)$ and $\psi_c(t)$.

$$\psi_a(t)_{j1} = \phi(2^{j1+1}t) + \phi(2^{j1+1}(t-1-2^{-(j1+1)})) \quad (24)$$
$$\psi_b(t)_{j2} = \phi(2^{j2+1}t) + \phi(2^{j2+1}(t-1-2^{-(j2+1)})) \quad (25)$$
$$\psi_c(t)_{j3} = \phi(2^{j3+1}t) + \phi(2^{j3+1}(t-1-2^{-(j3+1)})) \quad (26)$$

where $j1 = 1, 2, \ldots\ldots, j; j1 \in Z$,

$$j2 = j1 + (J-3), \quad j2 \in Z \quad (27)$$
$$j3 = j1 + (J-2), \quad j3 \in Z \quad (28)$$

$\phi(2^j t)$ is the Haar scaling function.

In the synthesis part, three reference signals can be recovered from their groups of samples using synthesis basis functions, produced as dilated and shifted versions of the following three dual scale-based linearly-combined synthesis scaling functions.

$$\check{\psi}_a(t)_{j1} = \phi(t) - \phi_a(t)_{j1} \quad (29)$$
$$\check{\psi}_b(t)_{j1} = \phi(t) - \phi_a(t)_{j2} \quad (30)$$
$$\check{\psi}_c(t)_{j1} = \phi(t) - \phi_a(t)_{j3} \quad (31)$$

The output voltages three-phase six-pulse wavelet modulated inverters are trains of amplified, dilated, and shifted versions of the synthesis basis functions. It allows output voltages to be expressed in terms of $\check{\psi}_a(t)$, $\check{\psi}_b(t)\check{\psi}_c(t)$ as in equations (29)-(31). This is an advantage of wavelet modulated inverter, compared to other inverters. Fig. 4. Shows the flowchart for generating switching pulses for three-phase WM inverter.

B. FRAME ANGLE CONTROL TECHNIQUE

In [35] resolution level control technique is proposed for controlling the output voltages of voltage source inverter, by adjusting the maximum of scale J, to produce a phase-shift angle θ. The resolution-level control showed good performance in terms of dynamics, stability, responsiveness, and accuracy. But as J being an integer, continuous adjustment of the output voltage cannot be achieved accurately, through controlling J. To overcome this limitation, frame angle control is used with wavelet modulated inverter [42].

The phasor diagram of v_{wa}, v_{wb}, v_{wc} produced by GSC, along with their $d-q$ axis components are shown in Fig. 5.

This frame angle θ is defined as,

$$\theta = \tan^{-1}\left(\frac{v_{wq}}{v_{wd}}\right) \quad (32)$$

Based on the frame angle θ, the reference signals $S_{ga}(t)$, $S_{gb}(t)$, $S_{gc}(t)$, are given as,

$$S_{ga}(t) = \sin(2\pi f_0 t - \theta) \quad (33)$$
$$S_{gb}(t) = \sin(2\pi f_0 t - (2\pi/3) - \theta) \quad (34)$$

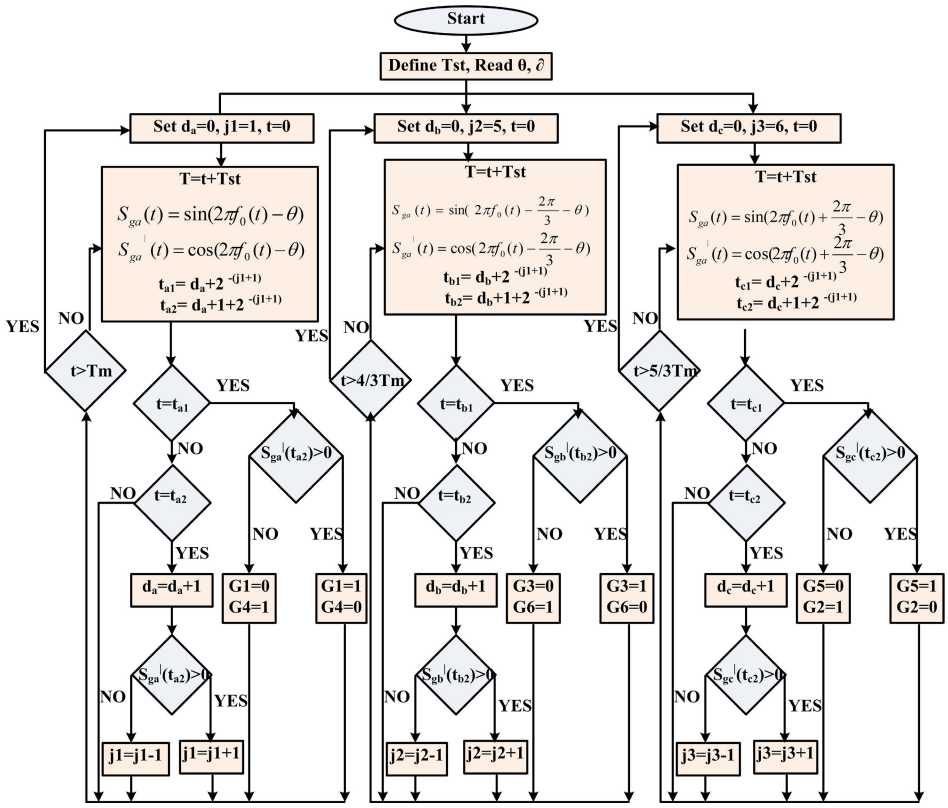

FIGURE 5. Flowchart for generating switching pulses for three phase WM inverter of the proposed WECS.

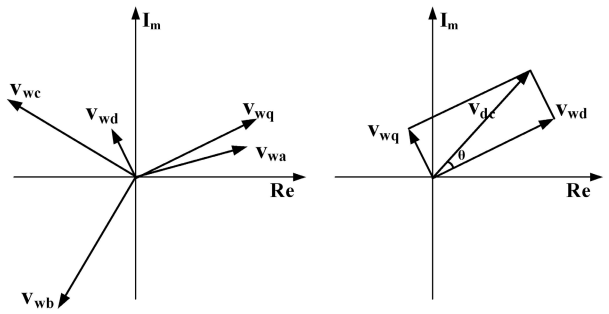

FIGURE 6. Phasor diagram to obtain the frame angle of the proposed WECS.

$$S_{gc}(t) = \sin(2\pi f_0 t + (2\pi/3) - \theta) \tag{35}$$

From the phasor diagram, d-q axis components of J (J∈Z) are related to v_{wd} and v_{wq} as,

$$v_{wd} = J_d v_{dc} \tag{36}$$

$$v_{wq} = J_q v_{dc} \tag{37}$$

where $j_d \in R$ and $j_q \in R$ are given as,

$$J_d = J\cos\theta \tag{38}$$

$$J_q = J\sin\theta \tag{39}$$

The variation of J_d and J_q with the values of i_{wd} and i_{wq} will vary the value of frame angle θ, which can control the output voltages of three-phase wavelet modulated GSC. This can allow the system to inject desired current to the grid and the load, depending on the input.

IV. RESULTS AND DISCUSSIONS

The effectiveness of the system is tested using MATLAB Simulink and experimental validation is done with the help of developed laboratory prototype. The laboratory arrangement is shown in Fig. 7.

A. STEADY-STATE BEHAVIOR OF WECS

The system is trained for a set of wind speeds to work at an optimum power coefficient of 0.48 and an optimum tip speed ratio of 8.1. The MSC makes the generator to work at unity power factor. Fig. 8. and Fig. 9. shows the test results of the proposed WECS for wind speed of 8 m/s. Fig. 8. shows the voltage and current waveform of the generator, voltage total harmonic distortion (THD), current THD, power values, and the DC link voltage. From these results, one can observe that the generator current and voltage are in phase and current total harmonic distortion (THD) is less than 5%.

In Fig.9. the performance of the WECS is analysed for performance under non-linear load conditions. The load THD is 20.7%, as in Fig. 9 (d). The GSC supplies a current of 1.216 A and grid supplies a current of 1.682 A as Fig (a) and (b), the load current harmonics is compensated by current injected by GSC, the source current THD is reduced to 4.6%.

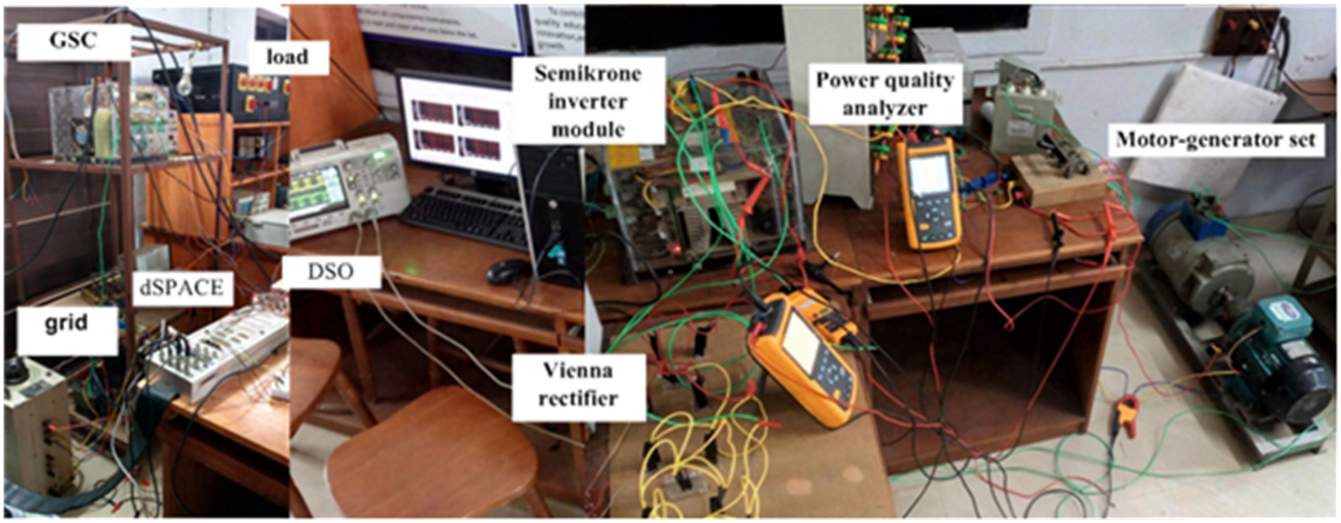

FIGURE 7. Experimental set-up.

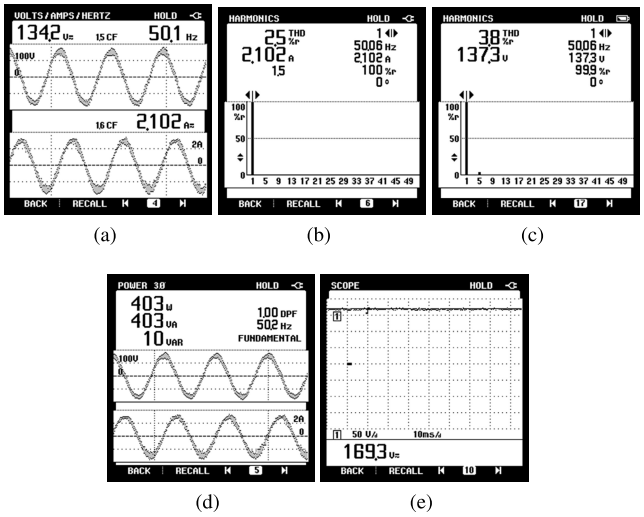

FIGURE 8. Experimental results of MSC at a wind speed of 8 m/s. (a) voltage and current (b) current THD (c) voltage THD (d) power waveforms (e) dc voltage.

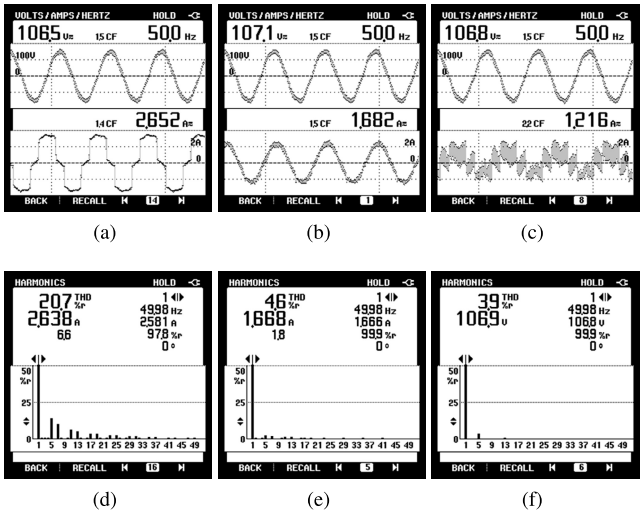

FIGURE 9. Voltage and current waveforms (a) load (b) grid (c) GSC,THD of (d) load current (e) grid current (f) grid voltage.

B. DYNAMIC PERFORMANCE OF WECS AT CHANGE IN WIND SPEED

For studying the performance of WECS, the system is checked for step changes in wind speed from 8 m/s-10m/s, 11m/s-12 m/s-10 m/s-8.5 m/s.

Fig. 10. shows the variation of power coefficient (Cp), output power, and generator speed with wind speed variation. For the changes in wind speed Cp value remains at the optimal value of 0.48. The power output at various wind speed increases with wind speed to its maximum value. The stator voltages and stator currents of PMSG for varying wind speed are depicted in Figure 11. From the enlarged view in Figure 11(c) and Figure 11(d), it is clear that the voltage and current settle to its new value within 0.01 sec. The voltage and current remain sinusoidal for all wind speeds within the range. For a constant load, the performance of WECS is verified for step changes in wind speed. When the wind speed is 8 m/sec, the major part of the active power of the load is supplied from the grid and a small portion is from WECS. When the wind speed increases to 10 m/sec, the supply from WECS increases as in Figure 12 (c), which indicates the direct-axis (d-axis) component of current injected by WECS. When wind speed reaches 12 m/sec, the d-axis component of the grid current is minimum and that of WECS is maximum. For all wind speeds the quadrature axis component of load current is completely met by WECS, making the grid current to work at unity power factor.

1) PERFORMANCE OF SYSTEM WITH VARIATION IN WIND SPEED

The dynamic performance of the system has been validated for a change in wind speed from 10 m/s to 8 m/s and the

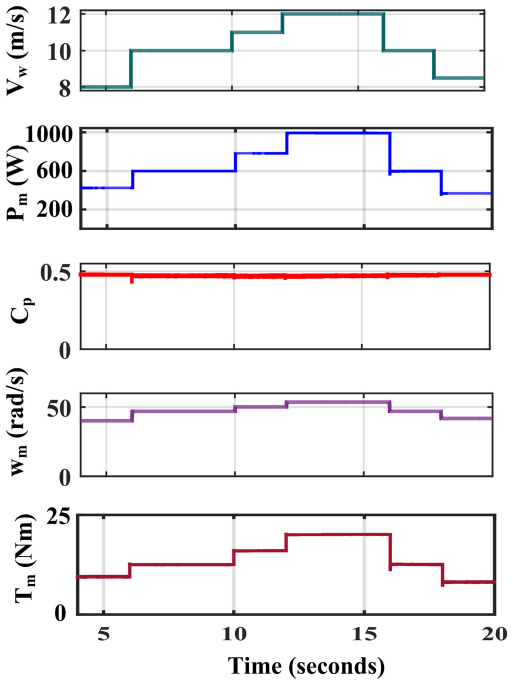

FIGURE 10. Performance of generator for step changes in wind speed (a) wind speed (m/s) (b) power coefficient (c) power output (W) (d) generator speed (rad/s).

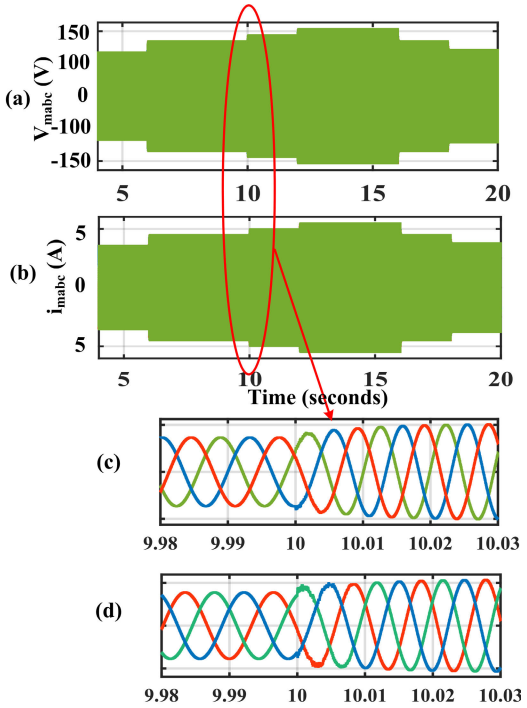

FIGURE 11. Performance of generator for step changes in wind speed (a) PMSG line voltages (V) (b) PMSG line currents (A) (c) Enlarged view of PMSG line voltages (V) (d) Enlarged view of PMSG line currents (A).

results are depicted in Figs. 13 (a)-(c). Fig. 13 (a) shows the variation of grid current in three phases i_{ga}, i_{gb}, i_{gc}, with change in wind speed, for a constant non-linear load. With the change in wind speed, grid current changes, and it gives a fast-dynamic response. Fig. 13 (b) shows the effect of

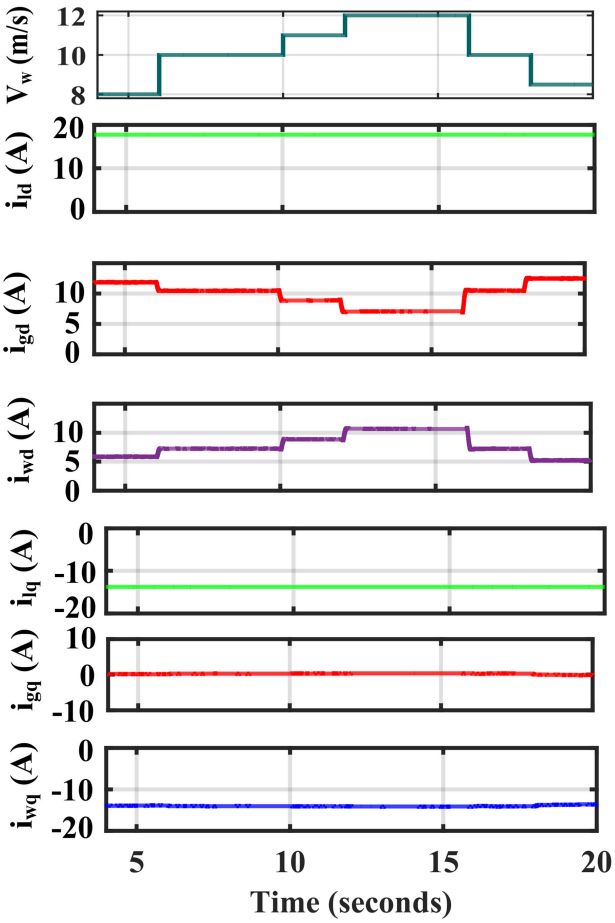

FIGURE 12. Grid side parameter variations with changes in wind speed (a) wind speed (m/sec) (b) d-axis component of load current (c) d-axis component of grid current (d) d-axis component of current injected by WECS (e) q-axis component of load current (f) q-axis component of grid current (g) q-axis component of current injected by WECS.

variations in wind speed on the grid current i_{ga}, GSC current i_{wa} and load current i_{la}. The increase in power generation from WECS, results in an increase in power supplied to the grid, which is visible in Fig. 11 (b) (grid current increases). Even though the load used is non-linear, the grid current is balanced and sinusoidal. The required amount of reactive power to the load is supplied from WECS, to keep the grid current with the unity power factor. Fig. 13 (c) shows the result of a decrease in wind power generation. Both during the increase and decrease of wind speed, the system shows satisfactory dynamic performance. When the wind speed increases, the SRWNN control technique generates new reference generator current (i^*_{md}) as shown in Fig. 13 (d). The corresponding current is tracked by PMSG, which confirms the effectiveness of the SRWNN control. It also shows that speed PMSG rotor changes in accordance with wind speed variation.

2) PERFORMANCE OF SYSTEM AT LOAD SIDE VARIATIONS

The system behaviour during the load variation is addressed in this section with the help of experimental results shown in

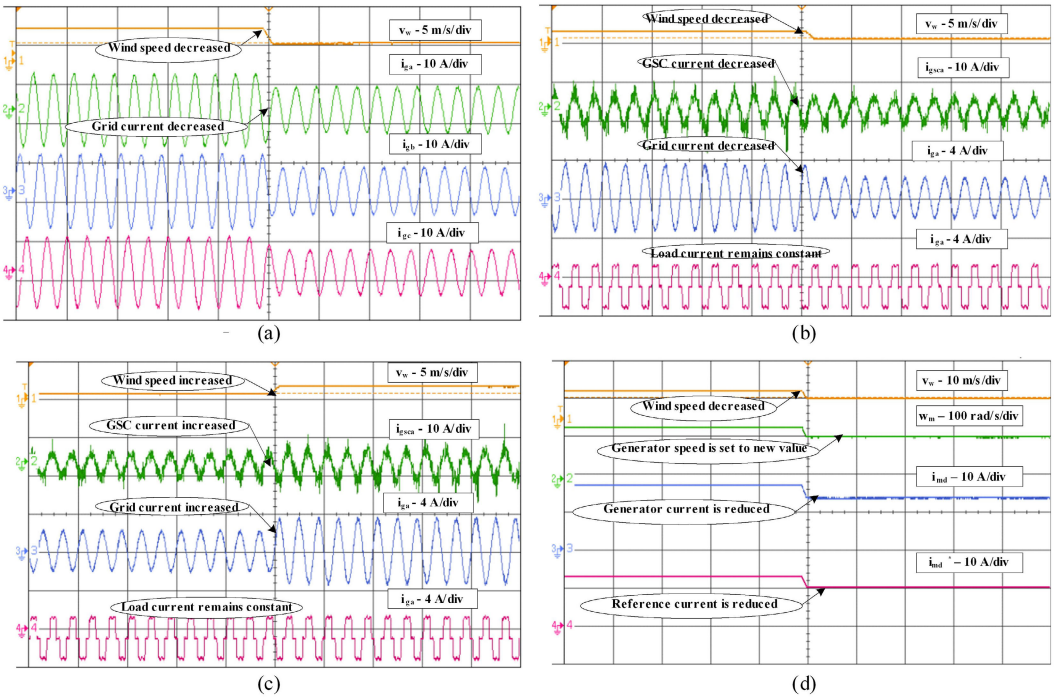

FIGURE 13. Dynamic performance of WECS on variation in wind speed (a) grid current variation for step changes in wind speed (b) grid current, current injected by WECS and load current for step increase in wind speed (c) grid current, current injected by WECS and load current for step decrease in wind speed (d) generator speed, reference d-axis current, actual d-axis current of PMSG for step changes in wind speed.

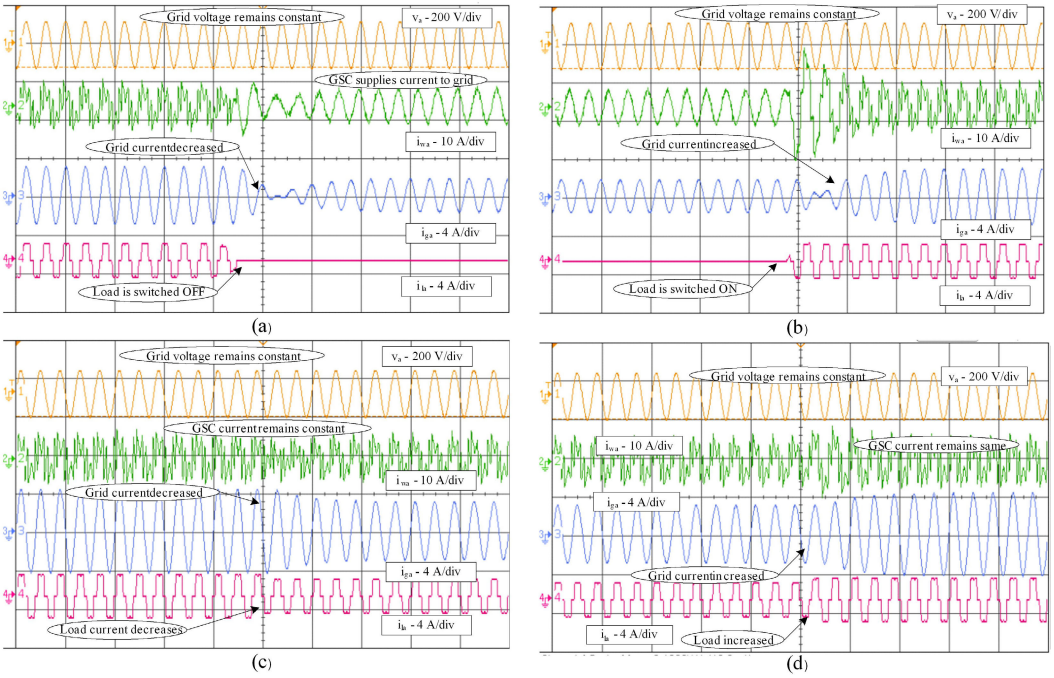

FIGURE 14. Dynamic performance of WECS for variation in load demand (a) grid current, current injected by WECS and load current for increase in load demand (b) grid current, current injected by WECS and load current for decrease in load demand (c) grid current, current injected by WECS and load current when the load is switched OFF (d) grid current, current injected by WECS and load current when the load is switched ON.

Figs. 14 (a)-(d). The system is analysed for a sudden rise in load demand and a sudden decrease in load demand.

Figs. 14 (a) and (b) show the performance of the system for a sudden increase and decrease in local load demand. A fast dynamic response is achieved during the change in load demand. With the power generated from WECS remaining the same, any change in load power directly affects the power flowing into the grid. When the load is absent, the total power

generated by WECS is transferred to the grid. When load appears, reactive power requirements of the load is met by GSC, and it acts as an active filter. The case when the load is switched OFF the power from WECS is supplied to the grid. At that time, there is no reactive power produced by WECS and the current injected by WECS is sinusoidal. The variation of grid current and WECS current during switching ON and switching OFF of the load is shown in Fig. 14 (c) and 14 (d). The system response parameters of SRWNN MPPT control is compared with Radial basis function (RBFN) MPPT control [25]. It is worthy to mention here that the steady-state error and settling time using the SRWNN MPPT control are lower than that achieved when the RBFN-based MPPT control is used as in Table 2. The performance of the system with frame angle control with WM is compared with the synchronous reference frame(SRF) control with carrier-based PWM [25]. Table 3. gives the performance parameters and it shows that there is a significant increase in the active power and reactive power delivered to the load with the proposed control.

TABLE 2. Comparison of SRWNN MPPT control with RBFN MPPT control.

System Response	Specification	SRWNN MPPT Control	RBFN MPPT Control [25]
Power output of PMSG	Steady-state error (percentage)	2	4.5
	Settling time (sec)	1.01	1.08
Rotor speed of PMSG	Steady-state error (percentage)	5	7
	Settling time (sec)	1.04	1.1
Real power of GSC	Steady-state error (percentage)	3	5
	Settling time (sec)	1.05	1.11
Reactive power of GSC	Steady-state error (percentage)	3.01	5
	Settling time (sec)	1.02	1.15

TABLE 3. Performance comparison of frame-angle control and SRF control.

Parameters	Frame angle-based		SRF control [25]	
Wind speed	10 m/sec	12 m/sec	10 m/sec	12 m/sec
Active power output from WECS	599 W	984 W	469 W	921 W
Reactive power output of the WECS	102 W	102 W	82 W	84 W
Active power output from grid	500 W	116 W	630 W	178 W
Reactive power output of the grid	0 W	0 W	25 W	21 W
THD of grid current (percentage)	<2.5	<2.5	(2.5- 5)	(2.5-5)
THD of grid voltage (percentage)	<2	<2	(2.5- 5)	(2.5-5)

V. CONCLUSION

A sensor-less wavelet neural network-based improved UPF rectifier for a WECS consists of a permanent magnet synchronous generator is proposed in this paper. The MSC using a Vienna rectifier with SRWNN control is tested for maximum power tracking, and the results prove that it is a useful technique with the fast-dynamic response for wind speed variations. It makes the WECS operates at an optimal power coefficient. The main advantages of the proposed system are,

- The system avoids the use of mechanical sensors for maximum power tracking.
- SRWNN MPPT control provides a fast-dynamic response to wind speed variations.
- Ensures unity power factor operation at generator and grid side.

Test results have also verified the frame-angle based control of wavelet modulated GSC to illustrate its improved PQ performance for local nonlinear load and to regulate the effective power delivery to the grid under changes in the wind speed or changes in load demand. The fame-angle control makes the WECS supplies the reactive power requirement of local load and makes the grid current at a unity power factor. Experimental analysis is conducted during steady-state and dynamic operating conditions.

APPENDIX

System Configuration:

The wind emulator consists of a DC motor with a DC drive coupled to PMSG. The wind emulator is connected to the grid/autotransformer through Vienna rectifier and a Semikron IGBT module as GSC. The MATLAB Simulink model is interfaced with the dSPACE 1104 controller to produce gate pulses. dSPACE controller is having an MPC8240 processor with PPC 603e core and on-chip peripherals. The gate pulses from the the dSPACE controller are connected to the converters through 6N136 gate driver circuit. The parameters of different components of WECS are shown in Table 4.

TABLE 4. Parameters of experimental prototype of WECS.

DC Motor	
Output Power	3hP
Nominal field voltage	220 V DC
Nominal armature voltage	220 V DC
DC Drive	
Input voltage	230 V
Input current	13 A
Output voltage	200 V DC
Output current	15 A
Switching frequency	10 kHz
PMSG	
Rated power	1kW
Rated terminal voltage	180 V
Rated frequency	50 Hz
Pair of poles	4
Stator resistance	0.52 Ω/phase
Stator inductance (Ld = Lq)	3.35 mH/phase
MSC	
Line inductance	5 mH
DC link Capacitance (C1=C2)	22 μF
Hysteresis band	0.1
GSC	
Proportional constant Kp	0.4
Integral constant Ki	0.23
Grid	
PCC voltage	110 V, 50Hz
Ripple filter (Rf, Cf)	2.5 Ω, 10 μF

ACKNOWLEDGMENT

The authors express their gratitude to the Centre of Excellence in Systems Energy and Environment (CESEE), Government College of Engineering, Kannur, India, for providing technical support and experimental platform.

The authors would also like to express their sincere gratitude to Renewable Energy Research Lab, College of Engineering, Prince Sultan University, Riyadh, Saudi Arabia, for providing technical inputs and reviews.

The support from Vimal Jyothi Engineering College, Chemperi, Kannur, India is also acknowledged.

REFERENCES

[1] Y.-K. Wu, W.-H. Yang, Y.-L. Hu, and P. Q. Dzung, "Frequency regulation at a wind farm using time-varying inertia and droop controls," *IEEE Trans. Ind. Appl.*, vol. 55, no. 1, pp. 213–224, Jan. 2019.

[2] C. Lumbreras, J. M. Guerrero, D. Fernandez, D. D. Reigosa, C. Gonzalez-Moral, and F. Briz, "Analysis and control of the inductorless boost rectifier for small-power wind-energy converters," *IEEE Trans. Ind. Appl.*, vol. 55, no. 1, pp. 689–700, Jan. 2019.

[3] J.-S. Lee and K.-B. Lee, "Predictive control of vienna rectifiers for PMSG systems," *IEEE Trans. Ind. Electron.*, vol. 64, no. 4, pp. 2580–2591, Apr. 2017.

[4] M. A. Soliman, H. M. Hasanien, H. Z. Azazi, E. E. El-Kholy, and S. A. Mahmoud, "An adaptive fuzzy logic control strategy for performance enhancement of a grid-connected PMSG-based wind turbine," *IEEE Trans. Ind. Informat.*, vol. 15, no. 6, pp. 3163–3173, Jun. 2019.

[5] Z. Zhang, F. Wang, J. Wang, J. Rodriguez, and R. Kennel, "Nonlinear direct control for three-level NPC Back-to-Back converter PMSG wind turbine systems: Experimental assessment with FPGA," *IEEE Trans. Ind. Informat.*, vol. 13, no. 3, pp. 1172–1183, Jun. 2017.

[6] V. Yaramasu, A. Dekka, M. J. Durán, S. Kouro, and B. Wu, "PMSG-based wind energy conversion systems: Survey on power converters and controls," *IET Electr. Power Appl.*, vol. 11, no. 6, pp. 956–968, Jul. 2017.

[7] J. Adhikari, P. I. V. G. Ponraj, and S. K. Panda, "Modeling, design, and implementation of a power conversion system for small-scale high-altitude wind power generating system," *IEEE Trans. Ind. Appl.*, vol. 53, no. 1, pp. 283–295, Jan. 2017.

[8] J.-S. Lee, K.-B. Lee, and F. Blaabjerg, "Predictive control with discrete space-vector modulation of vienna rectifier for driving PMSG of wind turbine systems," *IEEE Trans. Power Electron.*, vol. 34, no. 12, pp. 12368–12383, Dec. 2019.

[9] O. Aissa, S. Moulahoum, and B. Babes, "Functioning ability of multilevel vienna converter as new parallel active filtering configuration: Simulation and experimental evaluation," *Electr. Eng.*, vol. 101, no. 4, pp. 1103–1117, Dec. 2019.

[10] O. Aissa, S. Moulahoum, I. Colak, B. Babes, and N. Kabache, "Design and real time implementation of three-phase three switches three levels vienna rectifier based on intelligent controllers," *Appl. Soft Comput.*, vol. 56, pp. 158–172, Jul. 2017.

[11] M. Jahanpour-Dehkordi, S. Vaez-Zadeh, and J. Mohammadi, "Development of a combined control system to improve the performance of a PMSG-based wind energy conversion system under normal and grid fault conditions," *IEEE Trans. Energy Convers.*, vol. 34, no. 3, pp. 1287–1295, Sep. 2019.

[12] A. Beddar, H. Bouzekri, B. Babes, and H. Afghoul, "Real time implementation of improved fractional order proportional-integral controller for grid connected wind energy conversion system," *Rev. Roum. Sci. Tech. Électrotech. Energy*, vol. 61, 4, pp. 402–407, 2016.

[13] L. Guo, X. Zhang, S. Yang, Z. Xie, L. Wang, and R. Cao, "Simplified model predictive direct torque control method without weighting factors for permanent magnet synchronous generator-based wind power system," *IET Electr. Power Appl.*, vol. 11, no. 5, pp. 793–804, May 2017.

[14] A. Shafiei, B. M. Dehkordi, A. Kiyoumarsi, and S. Farhang, "A control approach for small-scale sc-based WECS in the whole wind speed range," *IEEE Trans. Power Electron.*, vol. 32, no. 12, pp. 9117–9130, Dec. 2017.

[15] M. B. Hemanth Kumar, B. Saravanan, P. Sanjeevikumar, and F. Blaabjerg, "Review on control techniques and methodologies for maximum power extraction from wind energy systems," *IET Renew. Power Gener.*, vol. 12, no. 14, pp. 1609–1622, Oct. 2018.

[16] S. Chatterjee and S. Chatterjee, "Review on the techno-commercial aspects of wind energy conversion system," *IET Renew. Power Gener.*, vol. 12, no. 14, pp. 1581–1608, Oct. 2018.

[17] I. U. Haq, Q. Khan, I. Khan, R. Akmeliawati, K. S. Nisar, and I. Khan, "Maximum power extraction strategy for variable speed wind turbine system via neuro-adaptive generalized global sliding mode controller," *IEEE Access*, vol. 8, pp. 128536–128547, 2020.

[18] M. Nasiri, J. Milimonfared, and S. H. Fathi, "Modeling, analysis and comparison of TSR and OTC methods for MPPT and power smoothing in permanent magnet synchronous generator-based wind turbines," *Energy Convers. Manage.*, vol. 86, pp. 892–900, Oct. 2014.

[19] J. Lee and Y.-S. Kim, "Sensorless fuzzy-logic-based maximum power point tracking control for a small-scale wind power generation systems with a switched-mode rectifier," *IET Renew. Power Gener.*, vol. 10, no. 2, pp. 194–202, Feb. 2016.

[20] M. A. Abdullah, T. Al-Hadhrami, C. W. Tan, and A. H. Yatim, "Towards green energy for smart cities: Particle swarm optimization based MPPT approach," *IEEE Access*, vol. 6, pp. 58427–58438, 2018.

[21] N. Priyadarshi, S. Padmanaban, M. Sagar Bhaskar, F. Blaabjerg, and A. Sharma, "Fuzzy SVPWM-based inverter control realisation of grid integrated photovoltaic-wind system with fuzzy particle swarm optimisation maximum power point tracking algorithm for a grid-connected PV/wind power generation system: Hardware implementation," *IET Electr. Power Appl.*, vol. 12, no. 7, pp. 962–971, Aug. 2018.

[22] B. Babes, L. Rahmani, A. Chaoui, and N. Hamouda, "Design and experimental validation of a digital predictive controller for variable-speed wind turbine systems," *J. Power Electron.*, vol. 17, no. 1, pp. 232–241, Jan. 2017.

[23] U. Abubakar, S. Mekhilef, H. Mokhlis, M. Seyedmahmoudian, B. Horan, A. Stojcevski, H. Bassi, and M. Hosin Rawa, "Transient faults in wind energy conversion systems: Analysis, modelling methodologies and remedies," *Energies*, vol. 11, no. 9, p. 2249, Aug. 2018.

[24] J. Hussain and M. K. Mishra, "An efficient wind speed computation method using sliding mode observers in wind energy conversion system control applications," *IEEE Trans. Ind. Appl.*, vol. 56, no. 1, pp. 730–739, Jan. 2020.

[25] D. Reddy and S. Ramasamy, "Design of RBFN controller based boost type vienna rectifier for grid-tied wind energy conversion system," *IEEE Access*, vol. 6, pp. 3167–3175, 2018.

[26] X. Deng, J. Yang, Y. Sun, D. Song, Y. Yang, and Y. H. Joo, "An effective wind speed estimation based extended optimal torque control for maximum wind energy capture," *IEEE Access*, vol. 8, pp. 65959–65969, 2020.

[27] F. F. M. El-Sousy and K. A. Abuhasel, "Intelligent adaptive dynamic surface control system with recurrent wavelet elman neural networks for DSP-based induction motor servo drives," *IEEE Trans. Ind. Appl.*, vol. 55, no. 2, pp. 1998–2020, Mar. 2019.

[28] H. A. Young, V. A. Marin, C. Pesce, and J. Rodriguez, "Simple Finite-Control-Set model predictive control of grid-forming inverters with LCL filters," *IEEE Access*, vol. 8, pp. 81246–81256, 2020.

[29] C. Wang, L. Yang, Y. Wang, Z. Meng, W. Li, and F. Han, "Circuit configuration and control of a grid-tie small-scale wind generation system for expanded wind speed range," *IEEE Trans. Power Electron.*, vol. 32, no. 7, pp. 5227–5247, Jul. 2017.

[30] F. Sebaaly, H. Vahedi, H. Y. Kanaan, and K. Al-Haddad, "Novel current controller based on MPC with fixed switching frequency operation for a grid-tied inverter," *IEEE Trans. Ind. Electron.*, vol. 65, no. 8, pp. 6198–6205, Aug. 2018.

[31] D. Thakur and J. Jiang, "Control of a PMSG wind-turbine under asymmetrical voltage sags using sliding mode approach," *IEEE Power Energy Technol. Syst. J.*, vol. 5, no. 2, pp. 47–55, Jun. 2018.

[32] S. M. Mozayan, M. Saad, H. Vahedi, H. Fortin-Blanchette, and M. Soltani, "Sliding mode control of PMSG wind turbine based on enhanced exponential reaching law," *IEEE Trans. Ind. Electron.*, vol. 63, no. 10, pp. 6148–6159, Oct. 2016.

[33] B. Singh, S. Kumar, and C. Jain, "Damped-SOGI-Based control algorithm for solar PV power generating system," *IEEE Trans. Ind. Appl.*, vol. 53, no. 3, pp. 1780–1788, May 2017.

[34] C. Zhang, X. Zhao, X. Wang, X. Chai, Z. Zhang, and X. Guo, "A grid synchronization PLL method based on mixed second-and third-order generalized integrator for DC offset elimination and frequency adaptability," *IEEE J. Emerg. Sel. Topics Power Electron.*, vol. 6, no. 3, pp. 1517–1526, Sep. 2018.

[35] S. A. Saleh and R. Ahshan, "Resolution-Level-Controlled WM inverter for PMG-based wind energy conversion system," *IEEE Trans. Ind. Appl.*, vol. 48, no. 2, pp. 750–763, Mar. 2012.
[36] S. A. Saleh, C. R. Moloney, and M. A. Rahman, "Analysis and development of wavelet modulation for three-phase voltage-source inverters," *IEEE Trans. Ind. Electron.*, vol. 58, no. 8, pp. 3330–3348, Aug. 2011.
[37] C. P. Archana, T. George, and P. Jayaprakash., "Wavelet modulated inverter for WECS using permanent magnet synchronous generator," in *Proc. IEEE Int. Conf. Power Electron., Drives Energy Syst. (PEDES)*, Chennai, India, Dec. 2018, pp. 1–5.
[38] S. A. Saleh, "On the performance of the frame-angle controller for 3ϕ interconnected PV systems," *IEEE Trans. Ind. Appl.*, vol. 55, no. 2, pp. 1189–1201, Mar./Apr. 2019.
[39] T. Friedli, M. Hartmann, and J. W. Kolar, "The essence of three-phase PFC rectifier systems—Part II," *IEEE Trans. Power Electron.*, vol. 29, no. 2, pp. 543–560, Feb. 2014.
[40] M. E. Haque, M. Negnevitsky, and K. M. Muttaqi, "A novel control strategy for a variable-speed wind turbine with a permanent-magnet synchronous generator," *IEEE Trans. Ind. Appl.*, vol. 46, no. 1, pp. 331–339, Jan. 2010.
[41] S. A. Saleh and M. A. Rahman, "Development and experimental validation of resolution-level controlled wavelet-modulated inverters for three-phase induction motor drives," *IEEE Trans. Ind. Appl.*, vol. 47, no. 4, pp. 1958–1970, Jul. 2011.
[42] S. A. Saleh and A. Rubaai, "Extending the Frame-Angle-Based direct torque control of PMSM drives to low-speed operation," *IEEE Trans. Ind. Appl.*, vol. 55, no. 3, pp. 3138–3150, May 2019.

TEENA GEORGE (Member, IEEE) was born in Kannur, Kerala, India. She received the B.Tech. degree in electrical and electronics engineering from the College of Engineering Trivandrum, Kerala University, India, in 2009, and the M.Tech. degree from the National Institute of Technology Calicut, India, in 2011. She is currently pursuing the Ph.D. degree with the Government College of Engineering, A. P. J. Abdul Kalam Technological University, Kannur. She has been working as an Assistant Professor with the Department of Electrical and Electronics, Vimal Jyothi Engineering College, Kannur, since 2011. Her research interests include renewable energy generation and power electronic controllers for power systems. She is a Life Member of the Indian Society for Technical Education (ISTE) and a member of the IEEE Power and Energy Society and Young Professionals. She is also a Reviewer Member of various international journals and conferences.

P. JAYAPRAKASH (Senior Member, IEEE) was born in Payyanur, India. He received the B.Tech. degree in electrical and electronics engineering from the University of Calicut, India, in 1996, and the M.Tech. degree in energy studies and the Ph.D. degree from the Indian Institute of Technology Delhi, New Delhi, India, in 2003 and 2009, respectively. He has worked as a Research Associate with the Integrated Rural Technology Centre, Palakkad, and as an Engineer with National Hydro Electric Power Corporation, Faridabad, India, from 1997 to 1998. He joined the Department, in 1999, and became an Associate Professor, in 2009. He has worked with the Dresden University of Technology, Dresden, Germany, for one year under DAAD Scheme, in 2003. He is currently a Professor with the Department of Electrical and Electronics Engineering, Government College of Engineering, Kannur, India. He has over 15 years of teaching experience. He has 18 journal publications and over 60 conference proceedings of reputed national/international conferences. His research interests include power quality, power electronics applications to power systems, and renewable energy. He is a Life Member of the Indian Society for Technical Education (ISTE). He is serving as a Reviewer for many IEEE and IET transactions and conferences. He is also serving as an Advisor for the IEEE IAS Chapter, Government College of Engineering, Kannur.

UMASHANKAR SUBRAMANIAM (Senior Member, IEEE) is currently with the Renewable Energy Laboratory, Department of Communications and Networks, College of Engineering, Prince Sultan University, Saudi Arabia. Previously, he worked as an Associate Professor, the Head of the VIT Vellore, a Senior Research and Development, and a Senior Application Engineer in the field of power electronics, renewable energy, and electrical drives. He has more than 16 years of teaching, research, and industrial research and development experience. He has published more than 250 research articles in national and international journals and conferences. He has also authored/coauthored/contributed 20 books/chapters and 15 technical articles on power electronics applications in renewable energy and allied areas. His research interest includes power electronics, sustainability, energy, and smart grid. He is a member of PES, PSES, and YP. He received the Danfoss Innovator Award-Mentor, from 2014 to 2015 and 2017 to 2018, the Research Award from VIT University, from 2013 to 2018. He was an Executive Member, from 2014 to 2016, and the Vice Chair of the IEEE MAS Young Professional, from 2017 to 2019. He held positions as the Vice Chair the IEEE Madras Section and the Chair of the IEEE Student Activities, from 2018 to 2019. He is an Editor of Heliyon, Springer Nature, and IEEE Access. He also received the INAE Summer Research Fellowship, in 2014. Under his guidance, 24 postgraduate students and more than 25 undergraduate students completed the senior design project work, and six Ph.D. scholars completed doctoral thesis as a Research Associate. He is also involved in collaborative research projects with various international and national level organizations and research institutions.

DHAFER J. ALMAKHLES (Senior Member, IEEE) received the B.E. degree in electrical engineering from the King Fahd University of Petroleum & Minerals (KFUPM), Dhahran, Saudi Arabia, in 2006, and the master's (Hons.) and Ph.D. degrees from The University of Auckland, New Zealand, in 2011 and 2016, respectively. Since 2016, he has been with Prince Sultan University, Saudi Arabia. He is currently an Assistant Professor with the Department of Communications and Networks Engineering. He is also serving as the Director of the Science and Technology Unit and the Leader of the Renewable Energy Laboratory, PSU. He has authored many published articles in the area of control systems. His research interests include the hardware implementation of control theory, signal processing, networked control systems, nonlinear control design, unmanned aerial vehicle (UAV), and renewable energy. He has served as a Reviewer for many journals, including the IEEE Transactions on Fuzzy Systems, the IEEE Transactions on Control of Network Systems, the IEEE Transactions on Industrial Electronics, the IEEE Transactions on Control Systems Technology, the IEEE Control Systems Letters, and the *International Journal of Control*.